93-GT-111

THE AMERICAN SOCIETY OF MECHANICAL ENGINEERS
345 E. 47th St., New York, N.Y. 10017

THREE-DIMENSIONAL ANALYSIS OF TURBINE ROTOR FLOW INCLUDING TIP CLEARANCE

R. Heider, J. M. Duboue, and B. Petot
Dept. of Turbo Aero and Cooling
Snecma
Moisssy-Cramayel, France

G. Billonnet
Department of Energetics
ONERA
Chatillon, France

V. Couaillier and N. Liamis
Department of Aerodynamics
ONERA
Chatillon, France

ABSTRACT

A 3D Navier-Stokes investigation of a high pressure turbine rotor blade including tip clearance effects is presented.

The 3D Navier-Stokes code developed at ONERA solves the three-dimensional unsteady set of mass-averaged Navier-Stokes equations by the finite volume technique. A one step Lax-Wendroff type scheme is used in a rotating frame of reference. An implicit residual smoothing technique has been implemented, which accelerates the convergence towards the steady state. A mixing length model adapted to 3D configurations is used.

The turbine rotor flow is calculated at transonic operating conditions. The tip clearance effect is taken into account. The gap region is discretized using more than 55,000 points within a multi-domain approach.

The solution accounts for the relative motion of the blade and casing surfaces. The total mesh is composed of five sub-domains and counts 710,000 discretization points. The effect of the tip clearance on the main flow is demonstrated. The calculation results are compared to a 3D inviscid calculation, without tip clearance.

NOMENCLATURE

C_p	specific heat coefficient
E	total specific energy
F	flux densities
$\overline{\overline{I}}$	identity tensor
K	Von Karman constant
Ma_r	relative Mach number
P	static pressure
Pt_r	relative stagnation pressure
Pr	Prandtl number
Pr_t	turbulent Prandtl number
$\overline{V}$	relative velocity
S	source terms
T	temperature
Tt_r	relative stagnation temperature
d	distance to walls
e	internal specific energy
f	conservative variables
l	mixing-length
q	heat flux
q_t	turbulent diffusion enthalpy flux
r	radius
s	reduced curvilinear abscissa
$\overline{\Omega}$	rotational speed
β	relative flow angle
γ	specific heat-coefficient ratio
δ	boundary layer thickness
λ	thermal conductivity
μ	molecular viscosity
μ_t	eddy viscosity
ρ	density
$\overline{\overline{\tau}}$	shear stress tensor
$\overline{\overline{\tau_R}}$	Reynolds tensor
ω	vorticity vector

Presented at the International Gas Turbine and Aeroengine Congress and Exposition
Cincinnati, Ohio — May 24–27, 1993

SUBSCRIPTS

1 inlet plane
2 analysis plane
is isentropic
bt blade tip
c casing
$\otimes$ tensorial product

INTRODUCTION

Numerical Methods for Turbomachinery Components Design

The use of advanced computational methods to improve performance of turbomachinery components as well as to reduce the design and development time and cost is very efficient. For a number of years, SNECMA has been spending much effort to include new design and analysis codes in its engine component development methodology.

Thus, ONERA and SNECMA have been working jointly on numerical methods for many years for the prediction of steady flows in turbomachinery.

The last step in the prediction of steady flows in turbine is achieved with the use of three-dimensional Navier-Stokes solvers. For purely aerodynamic cases such as those encountered in low pressure turbines, the quality of the flow field prediction is essentially dependent on the ability of the code to calculate accurate wall aerodynamics. This can be obtained relatively easily by the use of a viscous solver, a high level of discretization and a 'good' turbulence model. It was underlined by Chevrin and Vuillez (1990) and by Petot and Fourmaux (1992), that the mixing-length turbulence models give fairly accurate results for nominal working conditions at reasonable costs for turbine blade channel flows. This is confirmed by the results of Ameri and Arnone (1992) and those of Boyle and Giel (1992) for 2D and 3D flows including heat transfer predictions.

The work is much more complicated for highly cooled turbine blades for which the complete prediction of the flow field including film cooling and cooling injections is a task of major difficulty due to the complexity of the geometry but also of the flow which includes several scales of phenomena and very strong thermodynamic gradients. A step in this direction was recently accomplished by Dorney and Davis (1992). However, these promising results can give essentially qualitative information unless a very high level of discretization is used.

For quantitative results, 3D Navier-Stokes simulations already provide valuable information on the flow structure in blade channels, even when ignoring cooling flows. This was recently demonstrated on high pressure turbine stators by Wegener et al. (1992).

Numerical Approach

The solver used at SNECMA for the prediction of viscous flows in blade to blade channels was developed at ONERA and is described by Cambier and Escande (1990), Vuillot (1989) and Couaillier (1990).

For turbine flows the previous results were focused on the application of the code to stators by Escande and Cambier (1991). A calculation on a compressor rotor obtained using this code, was presented by Couaillier et al. (1991). A transonic fan blade was computed with the original two-step explicit scheme.

The most recent progress made at ONERA was obtained on the numerical method and led to an increase of robustness, accuracy and calculation time reduction. The numerical techniques are presented below in section I.

We choose to present the calculation of a high pressure turbine rotor flow with tip clearance. This geometry is highly loaded, the flow is transonic and weak shocks interact with the tip leakage flow.

Our purpose is to demonstrate the adequacy of the 3D Navier-Stokes analysis for the prediction, understanding and later optimization of blade tip geometry.

The simulation technique for the rotor with tip clearance is presented in Part II. Finally, the analysis of the results including the comparison with a 3D Euler calculation of the rotor without tip clearance are presented in part III.

Interest for the Flow in Unshrouded Rotors

The use of unshrouded rotors in highly loaded turbines is a widespread solution to obtain lower values of mechanical stresses in the blades. The drawback of this solution is related to the losses created by the leakage flow. In the same time, the tip of the blade has to be cooled by either injection in the groove or film cooling at the casing. The investigation of this very complicated flow region thus becomes a matter of prime importance.

The tip clearances in unshrouded rotors have been investigated for a long time by experimental means. The aim was to work out correlations predicting the influence of the tip clearance on the exit main flow or to validate simple models of the leakage flow. Several parameters describing this influence were retained as predominent. Among them the height of the gap compared to the height of the blade is obviously of most importance. The influence of other factors could be studied but a complete

description of the flow was impossible. Its detailed structure remained unknown until recent numerical work. A very complete overview of the state of the art of the latter approach was written by Booth (1985).

With the development of 3D Navier-Stokes solvers, the situation has changed, and the turbine designer can obtain, in the same time and at reasonable costs, a better knowledge of the influence of the tip clearance on the flow, and indicative data to improve the blade tip geometry. However, the optimization of the tip clearance remains mainly related to technological know-how and several studies on optimization have demonstrated the complexity of the task (Heyes et al., 1991).

A Short Overview of Numerical Tip Clearance Studies

Several numerical investigations have been performed recently for the study of tip clearance flows for either compressor or turbine rotors. The most frequently tested turbine geometries are highly loaded rotor blades.

The influence of tip clearance on the main flow is all the more important for low aspect ratio turbines as the clearance height cannot be decreased for technological reasons.

The study of Briley et al. (1991) on the high turning Generic Gas Generator Turbine rotor blade is representative of what can be done within this approach. For instance, the influence of an upstream backstep on the reduction of tip clearance losses is found to be negligible. This might be indicative that the leakage flow is essentially driven by shear stress due to the casing. The level of discretization is among the highest encountered in literature, but very little information is given on the gap meshing technique.

A thorough study of a low aspect ratio turbine with and without tip clearance has been performed by Choi and Knight (1991). Although the level of discretization seems low, interesting techniques have been developed concerning the grid generation, and a detailed analysis of the gap region is provided.

Another purpose of running 3D viscous calculations can be to build a numerical data base for the assessment and validation of tip leakage flow models used in simplified simulation approaches such as throughflow calculations. For this purpose the 3D results have to be detailed and accurate. The best way to obtain such numerical results is to discretize the geometry as precisely as possible. This was underlined by Perrin et al. (1991).

Various grid generation techniques have already been tried by several authors for the gap region discretization. The approaches for turbine and compressor blades are different as long as the blade thickness is to be considered as a major parameter. The simplest one is to use a single domain. This leads to highly skewed grid when describing the tip of the blade.

In recent works (Choi, 1992), turbine calculations with tip clearances were run on O type meshes wrapping around the blade, with an added inner domain in the gap region. This domain is either an H type or an O type grid. The latter offers an easy treatment of the continuity between inner and outer O domains. In the case of highly cambered blades, however, it leads to severely distorted grids.

Our approach for the tip clearance flow prediction is to use a highly refined grid able to stand the very strong gradients due to the relative motion of the blade and casing.

I CALCULATION TOOL

Physical Model

The physical model is the compressible mass averaged Navier-Stokes equations associated with an algebraic mixing-lengh turbulence model. The Navier-Stokes equations are written in a cartesian coordinate system *(x,y,z)* rotating with angular velocity $\bar{\Omega}$ around the *x*-axis as follows :

Continuity equation :

$$\frac{\partial \rho}{\partial t} + div\ (\rho \bar{V}) = 0$$

Momentum equation:

$$\frac{\partial \rho \bar{V}}{\partial t} + div\ (\rho \bar{V} \otimes \bar{V} + p\bar{\bar{I}}) = div\ (\bar{\bar{\tau}} + \bar{\bar{\tau}}_R) + \rho\,(\Omega^2 \bar{r} - 2\bar{\Omega} X\ \bar{V}) \quad (1)$$

Energy equation :

$$\frac{\partial \rho E}{\partial t} + div\ (\rho E \bar{V} + p\bar{V}) = div\ [(\bar{\bar{\tau}} + \bar{\bar{\tau}_r}).\bar{V} - \bar{q} - \bar{q_t}] + \rho\,\Omega^2 \bar{r}.\bar{V}$$

Assuming a perfect gas, the static pressure is given by the following law :

$$p = (\gamma - 1)\rho\,(E - \frac{1}{2}V^2), \quad (2)$$

where γ is the ratio of the constant specific heats.

Using Stokes' hypothesis, the shear stress tensor is given by the following expression :

$$\bar{\bar{\tau}} = -\frac{2}{3}\mu\,(div\bar{V})\,\bar{\bar{I}} + 2\mu\,\bar{\bar{D}} \quad (3)$$

where μ is the molecular viscosity calculated with the averaged internal energy, $\bar{\bar{I}}$ being the unit tensor and $\bar{\bar{D}}$ the following operator:

$$\bar{\bar{D}} = \frac{1}{2}(\nabla \bar{V} + \nabla \bar{V}^T) \quad (4)$$

The heat flux $\bar{q}$ is given by Fourier's law:

$$\bar{q} = -\lambda \nabla T = -\frac{Cp\,\mu}{Pr} \nabla T \tag{5}$$

where Pr is the Prandtl number assumed constant and equal to 0.72 and where the molecular viscosity is given by Sutherland's law.

The Reynolds tensor $\bar{\bar{\tau}}_R$ and the turbulent diffusion enthalpy flux $\bar{q}_t$ are given by the model of Michel et al. (1969).

$$\bar{\bar{\tau}}_R = -\frac{2}{3}\mu_t\,(div\bar{V})\,\bar{\bar{I}} + 2\mu_t\,\bar{\bar{D}} \tag{6}$$

$$\bar{q}_t = -\frac{Cp\,\mu_t}{Pr_t} \nabla T \tag{7}$$

where Pr_t is the turbulent Prandtl number commonly fixed at 0.9. The eddy viscosity μ_t is obtained as follows :

$$\mu_t = \rho l^2 F^2 |\bar{\omega}| \tag{8}$$

$$l = 0{,}085\,\delta\, th\,(\frac{K}{0{,}085}\cdot\frac{d}{\delta}) \tag{9}$$

where $K=0.41$ is the Von Karman constant. F is the Van Driest viscous sublayer damping function given by :

$$F(\xi) = 1 - \exp(-\frac{\sqrt{\xi}}{26K})$$

$$\text{where } \xi = \rho l^2 \frac{\mu+\mu_t}{\mu^2} |\bar{\omega}| \tag{10}$$

In equation (9), d is Buleev's "modified distance" which is used to account for the influence of several walls in corner flows, and δ is a "modified boundary layer thickness". Equations (8), (9) and (10) give an implicit equation for μ_t, which is solved by a Newton method.

In the following we use system (1), written in a more compact form :

$$\frac{\partial f}{\partial t} + div\,(F - F_v) = S\ , \tag{11}$$

where f denotes the conservative variables, F the flux densities corresponding to the convective terms, F_v the flux densities corresponding to the viscous terms and S denotes the source terms.

Numerical Scheme

The numerical scheme used to solve the system of equations considered here is an implicit scheme which can be decomposed in an explicit stage and an implicit stage. The explicit stage is based on the scheme proposed by Ni (1982), for the solution of the Euler equations in a fixed frame of reference. More precisely, the idea of "distribution formulae" introduced by Ni in a one step Lax-Wendroff type scheme is used to solve the Navier-Stokes equation system including source terms due to rotation. The implicit stage has been proposed by Lerat et al. (1983) for the Euler equations, and already used by Couaillier et al. (1992) for the Euler equations associated with the Ni scheme.

Explicit Ni scheme

We briefly recall the discretization that we use. More details, especially concerning the contour integral appearing in the following, are given by Billonnet et al. (1992).

Time discretization. We use a Lax-Wendroff time discretization scheme, where the solution f^{n+1}, at the time $t^{n+1} = t^n + \Delta t$ is obtained from the solution at time t^n by the following expression :

$$f^{n+1} = f^n - \Delta t\, div(F^n - F_v{}^n) + \Delta t\, S^n + \frac{\Delta t^2}{2} div[A^n . div\,(F^n - F_v{}^n)] + \frac{\Delta t^2}{2}\frac{\partial S^n}{\partial t} \tag{12}$$

where A is the Jacobian matrix of the convective fluxes. It corresponds to a first order time discretization in the viscous region and to a second order time discretization in the perfect flow region (Cambier et al., 1988). The scheme can be rewritten as follows :

$$\delta f^n = -\Delta t\, div(F^n - F_v{}^n) + \Delta t\, S^n \tag{13.a}$$

$$\delta^2 f^n = -\frac{\Delta t}{2} div(A^n . \delta f^n) + \frac{\Delta t^2}{2}\frac{\partial S^n}{\partial t} \tag{13.b}$$

$$f^{n+1} = f^n + \delta f^n + \delta^2 f^n \tag{13.c}$$

It has to be noted that if S_f is the function defined by $S = S_f(f)$, then the term $\partial S/\partial t$ is equal to $S_f(\delta f)$.

Space discretization. In the following, we denote by A, B, C, D, E, F, G, H, the eight mesh points defining the cell Ω_a the center of which is the point a, and by a, b, c, d, e, f, g, h, the eight centers of the cells surrounding the mesh point G and defining the staggered cell ω_G (fig. 1). The volumes of the cells Ω_a and ω_G are respectively denoted by $v(\Omega_a)$ and $v(\omega_G)$.

At each time step t^n, the solution f^n is known at each point of the mesh, and the space discretization of the one-step scheme (12) is made of the following three stages :

i) The calculation of $\nabla\bar{V}$ and ∇T, at each mesh point G, for the evaluation of the viscous term at time t^n is performed as follows :

$$\nabla\bar{V}_G = \frac{1}{v(\omega_G)} \int_{\partial\omega_G} \bar{V}\,\bar{\otimes}\,\bar{n}\, dS \tag{14-a}$$

$$\nabla T_G = \frac{1}{v(\omega_G)} \int_{\partial\omega_G} T\,.\,\bar{n}\, dS \tag{14-b}$$

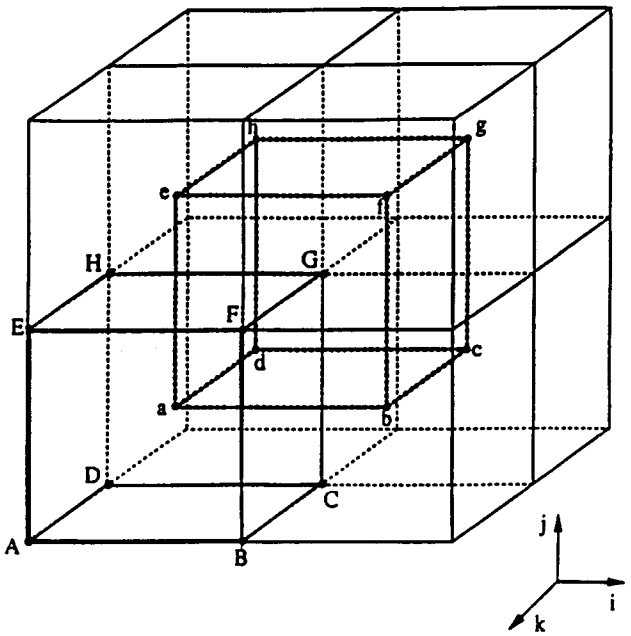

Fig. 1 : Notations for the spatial discretization

ii) The calculation of the first order term (13.a) at the cell centers is performed as follows :

$$\delta f_a = = \frac{-\Delta t}{v(\Omega_a)} \int_{\partial\Omega_a} (F - F_v).\bar{n}\, dS + \Delta t\, S_a{}^n \qquad (15)$$

The source term $S_a{}^n$ at point *a* is calculated from a mean value of the variable *f*. The first order term of (13.a) at mesh point *G* is obtained by taking the arithmetic mean of the values of δf computed at the cell centers *a, b, c, d, e, f, g, h*.

iii) The first order term values δf is known at the nodes for the calculation of the second order source term and at the barycenters of the cells for the calculation of $[div(A\delta f)]$. The second order term $\delta^2 f$ is directly determined at mesh point *G*.

Using the "distribution formulae" introduced by Ni, the scheme (12) can then be written :

$$f_G^{n+1} = f_G^n + \sum_a \left[\frac{\delta f_a}{8} - \frac{\Delta t}{2} (A\,\delta f)_a^n . \bar{N}_a{}^G \right] + \frac{\Delta t^2}{2} \left(\frac{\partial S^n}{\partial t} \right)_G , \qquad (16)$$

where the vector N_a is an expression which brings in only the cell geometry Ω_a.

The time step Δt used to integrate the solution in time with the scheme above is a local time step determined from the following formula which takes into account the convection and diffusion limitations :

$$\Delta t = \eta \min \left[\frac{h}{V + c} , \frac{\rho h^2}{2} / \gamma \left(\frac{\mu}{Pr} + \frac{\mu_t}{Pr_t} \right) \right] ,$$

where *h* is a characteristic length of the mesh cell, representing an evaluation of the dimension of the numerical dependence domain, *c* the local sound speed. η is a numerical coefficient which has to reflect the stability conditions for the convection part (CFL criterion) and for the diffusion part.

Artificial Viscosity. Due to the non dissipative property of the scheme in the sense of Kreiss, a fourth order linear dissipation D_4 is added. A second order non linear dissipation D_2 is also added in order to capture the flow discontinuities correctly. This treatment is analogous to that proposed by Jameson and Schmidt (1985) with a numerical boundary treatment introduced by Erikson (1984). Let us denote by $f^{n+1,E}{}_G$ the value of *f* obtained after the explicit stage (16); by adding the artificial viscosity we get a new value of *f* :

$$f^{n+1,ED}{}_G = f^{n+1,E}{}_G + \frac{\Delta t}{v(\omega_G)} [D_2(\varepsilon_2 . f^n) + D_4(\varepsilon_4 . f^n)]_G \qquad (17)$$

The coefficients ε_2 and ε_4 depend on the local geometry and on a sensor evaluating second differences of the local aerodynamic field. Because it is important to detect contact discontinuities, a combination of pressure and velocity differences is used.

Implicit stage

The implicit stage preserves the space centered approach, the conservative property, the accuracy and the dissipative (or non-dissipative) aspect of the explicit stage. This implicit stage consists in solving the following factorised operator (ADI technique) :

$$[\prod_{l=i,j,k} IS_l]\, R_G = R_G{}^* \qquad (18)$$

where $R_G{}^*$ and the operator IS_l are defined by:

$$R^*{}_G = f^{n+1,ED}{}_G - f^n{}_G \qquad (19)$$

$$IS_l = [1 + \frac{\beta_l}{2} \frac{\Delta t}{v(\omega_G)} \delta_l (\frac{\Delta t}{V} \rho^2 (A . n_l)\, \delta_l)] \qquad (20)$$

The space operator δ is defined by $\delta_l \Phi = \Phi_{l+1/2} - \Phi_{l-1/2}$, and $\rho(An_l)$ is the spectral radius of the matrix $A^n n_l$, n_l beeing the surface vector of the staggered cell in the *l* direction.

The parameters β_l are chosen in order to increase the stability domain. For the inviscid case, by a 3-D linear stability analysis of the Euler system of equations, assuming a cartesian and uniform grid, one can determinate their values ensuring the unconditional stability of the method. However, for the Navier-Stokes equations,

it is not possible to obtain unconditional stability by using this implicit stage. Nevertheless, the domain of stability is larger than by using only the explicit stage. To illustrate this fact, we consider the one-dimensional scalar equation :

$$\frac{\partial f}{\partial t} + a \frac{\partial f}{\partial x} = \nu \frac{\partial^2 f}{\partial x^2}$$

The domains of stability for the explicit scheme and for the implicit scheme are plotted on (fig. 2), where we have used the following relations :

$$A = a \frac{\Delta t}{\delta x} \ , \ N = \nu \frac{\Delta t}{\delta x^2} \ , \ s = -(\beta + \frac{1}{2}) \ ,$$

δx being the space step.

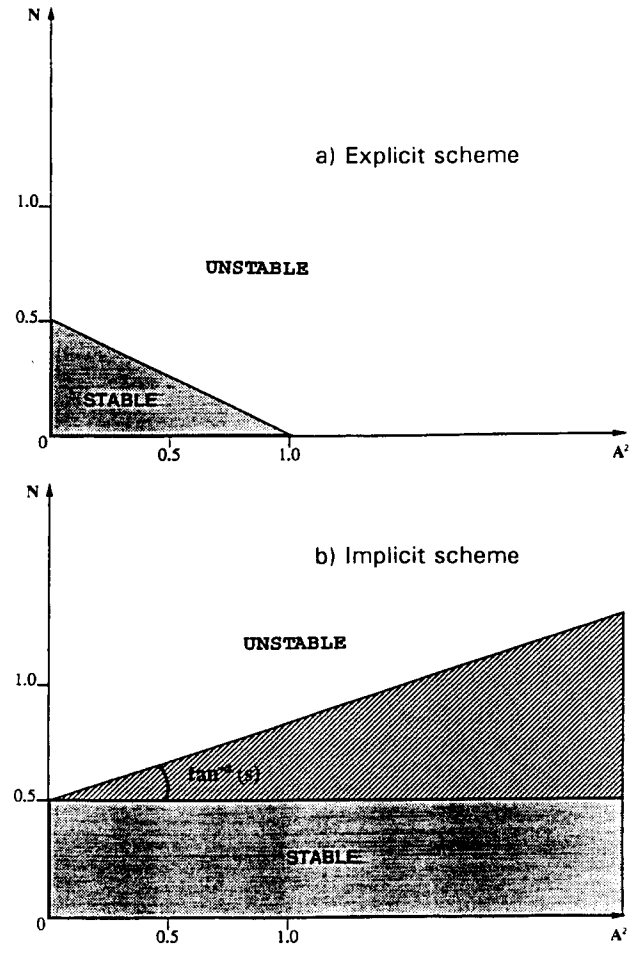

Fig. 2 : Stability domain

It is obvious that by using the implicit stage the stability domain becomes larger, and that the stability condition is controlled only by the dissipative term. For the 3-D calculations presented in this paper, the value of β_I ensuring stability and good convergence rate is equal to -1. The new value $f_G^{n+1,I}$ is obtained from the implicit stage as follows :

$$f_G{}^{n+1,I}{}_G = f^n{}_G + R_G \qquad (21)$$

We use fictitious points to apply the numerical boundary condition (of Neumann or Dirichlet type) on the residual R in the implicit stage.

Calculation time reduction

The (710200 grid points) calculation presented in part 2 has been performed twice. A first computation has been run using the purely explicit scheme, a second one with the implicit scheme.

For the explicit calculation, 20000 iterations with a time step factor of $\eta = 0.3$ were necessary to achieve convergence, characterized by a decrease of maximum residue of 3 orders of magnitude. The computation took 10 μs per iteration and point on a Cray YMP, resulting in total CPU run time of 40 hours.

For the computation using the implicit step, the run-time per iteration and grid point increased up to 12 μs. However a time step factor of $\eta = 3$ could be used and only 3000 iterations were necessary to achieve a similar degree of convergence. Hence, CPU run time could be reduced to only 7 hours for the same application.

II ADAPTATION TO TIP CLEARANCE CALCULATIONS

Grid Generation

Meshing of The Blade Channel. The computational domain is divided into five subdomains, each of which supports a structured grid. The approach chosen to generate the grid for a rotor with tip clearance is derived from the method employed for stators (Escande, 1991). A radially stacked mesh formed by 2-D H-O-H grid surfaces extends from hub to casing, thus leaving a gap in the tip clearance region (fig. 3).

The radial distribution of the 2-D surfaces is clustered near hub and casing to capture the endwall boundary-layers correctly. This distribution is interpolated from the streamlines predicted by a throughflow calculation. This in-house developed throughflow code not only provides streamlines for the mesh surfaces, but also aerodynamic data for boundary conditions and initial flow field.

On each of the so-defined axisymmetric surfaces, an H+O+H grid is generated. The O grid wrapping around the airfoil is created in three steps. At first, a coarse O grid is built using an algebraic mesh generator. A 2-D grid optimization using the method proposed by Jacquotte and Cabello (1988) is then performed on that grid to gain the essential properties of regularity and orthogonality.

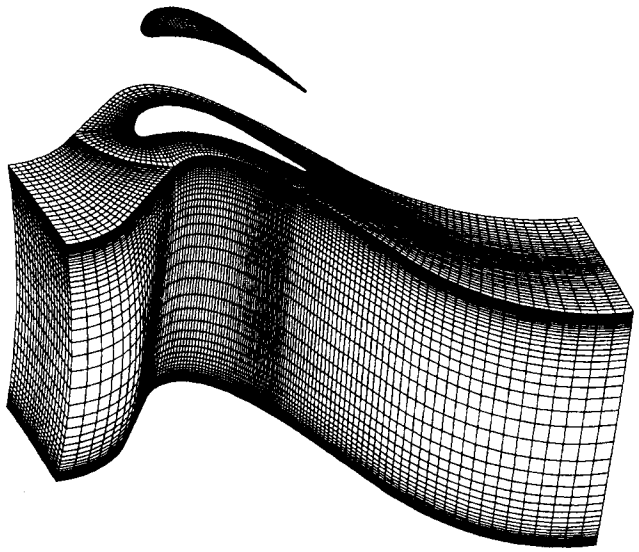

Fig. 3 : 3-D H+O+H Computational grid associated with an O+H grid describing the blade tip clearance geometry.

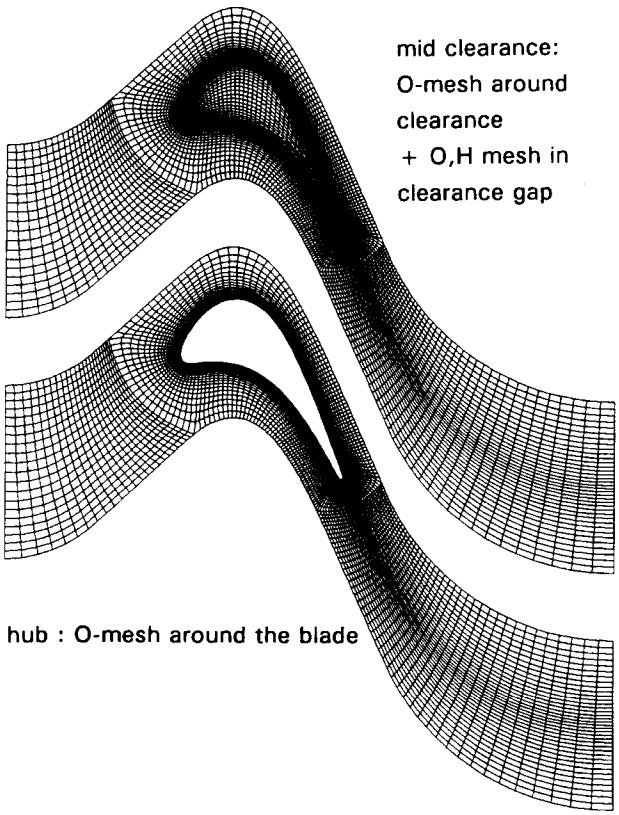

Fig. 4 : 2D stacked grid

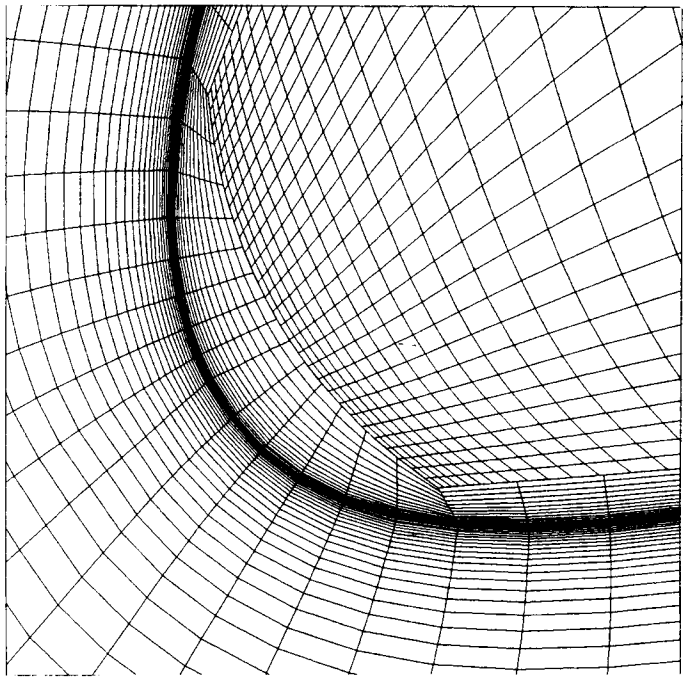

Fig. 5 : Detail of the leading edge in clearance zone figuring O channel grid and O+H clearance grid

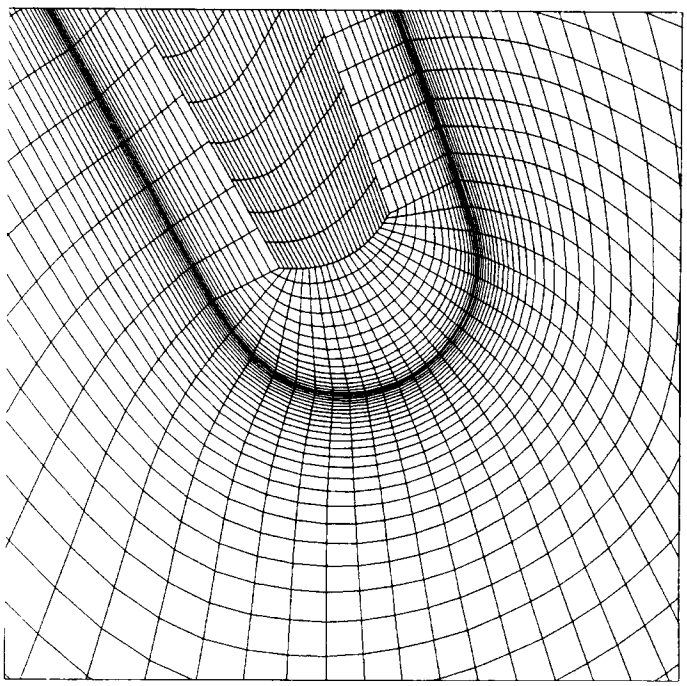

Fig. 6 : Detail of the trailing edge in clearance zone figuring O channel grid and O+H clearance grid

Hereafter, a denser grid clustered near the blade wall is interpolated on the coarse one to capture the boundary layers along the profile.

Meshing of the Tip Clearance. The gap left in the O-mesh between the blade tip and the casing is divided into two sub-domains formed by an O mesh leaning on the outer O-mesh described above, and an inner H-mesh (fig. 4). Both subdomains extend over 11 axisymmetric surfaces which are radially equidistant and stacked from the blade tip to the casing. Only the surface corresponding to the blade tip and the one corresponding to the casing coincide with the outer grid surfaces. On those two surfaces, the O-O interface has coinciding grid nodes. Since the mesh cell size at the inner O-H interface is larger than at the O-O boundary, it was not judged necessary to keep coinciding points there, although special care was paid to the regularity of the mesh in the whole tip region (fig. 5 and 6).

This two-domain grid of the gap region has the advantage of saving grid points in the central region of the clearance and to be well adapted to the next evolution in which the groove and its cooling injection will be taken into account. It was finally chosen after several tests on other types of grids such as those employed by Billonnet et al. (1992).

The total number of grid points is equal to 710,200 which divides into following $I*J*K$ distribution

25*21*67	upstream H zone
+185*41*67	channel O zone
+ 45*37*67	downstream H zone
+185*15*11	clearance O zone
+ 75*30*11	clearance H zone

Boundary Conditions

As stated before, the aerothermodynamic conditions result from a previous throughflow calculation. A radial distribution of stagnation pressure, stagnation temperature and flow angle is imposed upstream in the relative frame. Since the presence of the endwall viscous zones is not seen by a meridional calculation, an algebraic filter is applied to those distributions in order to take into account the influence of the boundary layers near the rotating hub and stationary casing (fig. 8).

Downstream, radial equilibrium and static pressure at mid-height are imposed during the first fifty iterations followed by a non-reflective condition to avoid shock reflexion due to imposed circumferentially uniform pressure.

An adiabatic, zero velocity condition is imposed on all wall surfaces. On the rotating ones, this condition is applied in the relative frame. At the casing, this is done in the absolute fixed coordinate system, followed by a variable transformation backward into the relative system.

Boundaries between subdomains are treated using trilinear interpolation on the unknowns. This technique does not imply matching grid nodes at the interface which greatly facilitates the meshing of complex geometries. However, trilinear interpolation being not conservative for non-matching points, the use of coinciding grid points is recommended in difficult areas such as the O-O interface in the clearance region. For such a curved boundary non-matching points would lead to holes between the boundaries and thus to interpolation errors. For other less curved boundaries the high level of discretization allows non matching grid points, the interpolation being precise enough.

Flow-Field Initialization

The initial flow field is obtained through interpolation of the calculation variables in the meridional flow field. The velocity vectors are then progressively deflected in order to be tangent to all solid surfaces. Filtering functions are applied to all rotating walls to simulate the rotating boundary layers. Near the casing, the relative velocity vectors are progressively turned into azimuthal direction to take the presence of the stationary casing into consideration.

Adaptation of the Turbulence Model

As stated above, the employed mixing length model requires computation of a typical distance to the wall and a boundary thickness δ. This can be done in a straightforward manner in the same way as exposed by Michel et al. (1969). In the clearance gap the modified distance d is taken to be

$$d = d_{bt}d_c/(d_{bt}+d_c) \qquad (22)$$

d_{bt} and d_c respectively being the distance from computation point to blade tip and to casing. Outside the clearance and near the casing in the surrounding O-zone, d is a combined function of the distance to the endwalls and to the tip edges of the suction and pressure side.

This approach ensures the continuity of the eddy viscosity.

Euler Calculation

The 3D Euler calculation was performed on the same geometry without clearance gap at identical operating conditions.

The 3D Euler code was already presented by Vuillot (1989) and Fourmaux and Petot (1991). From the

industrial standpoint, its ability to predict a part of the secondary flow in a low pressure stator when computing a flow with a non uniform radial distribution of stagnation pressure was underlined by Vialonga et al. (1992). A high density H-C mesh (more than 110,000 points) is chosen.

III ANALYSIS OF THE RESULTS

Geometry and Operating Conditions

The shape of the flowpath is conical at hub and cylindrical at the casing (fig. 7). The inlet conditions for both calculations stem from a throughflow calculation. The inlet plane is located at one axial chord upstream of the blade's leading edge. At this station, the inner radius of the flowpath is equal to 324.06 mm and the outer radius to 371.6 mm. The analysis plane is located at 25 % axial chord downstream of the blade trailing edge where the inner radius is equal to 319.32 mm and the outer radius to 371.6 mm. The gap height is taken to be 0.73 % of channel height which is equivalent to 0.36 mm.

The aerodynamic operating conditions are presented in table 1. The rotational speed is equal to 13500 rpm. The cooling of the blade tip is not modelled in this calculation.

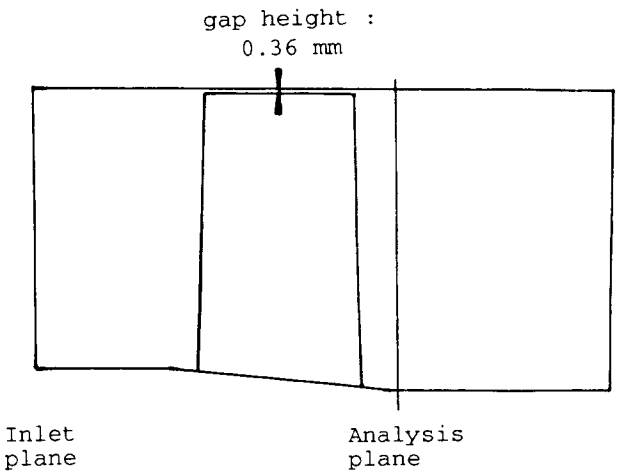

Fig. 7 : Meridional view of the flowpath

	Hub 10%	Mean 50%	Tip 90%
β_1 (deg)	60.20	60.20	53.70
Ma_{r1}	0.59	0.52	0.40
β_2 (deg)	-65.70	-67.50	-66.50
Ma_{r2}	1.06	1.13	1.11

Table 1 : Operating Conditions of the Blade. Throughflow predictions.

The inlet conditions are shown as radial evolutions on fig. 8. These distributions do not represent operating conditions such as those encountered downstream from a guide vane, but have been chosen almost uniform in order to obtain a better understanding of the basic phenomena. The deflection of the relative flow-angle at the tip, $\beta_1 = -90°$ represents the influence of the stationary casing. Therefore the relative stagnation pressure and temperature are sharply modified at the vicinity of the casing boundary-layer. This effect is of course not seen by the Euler calculation.

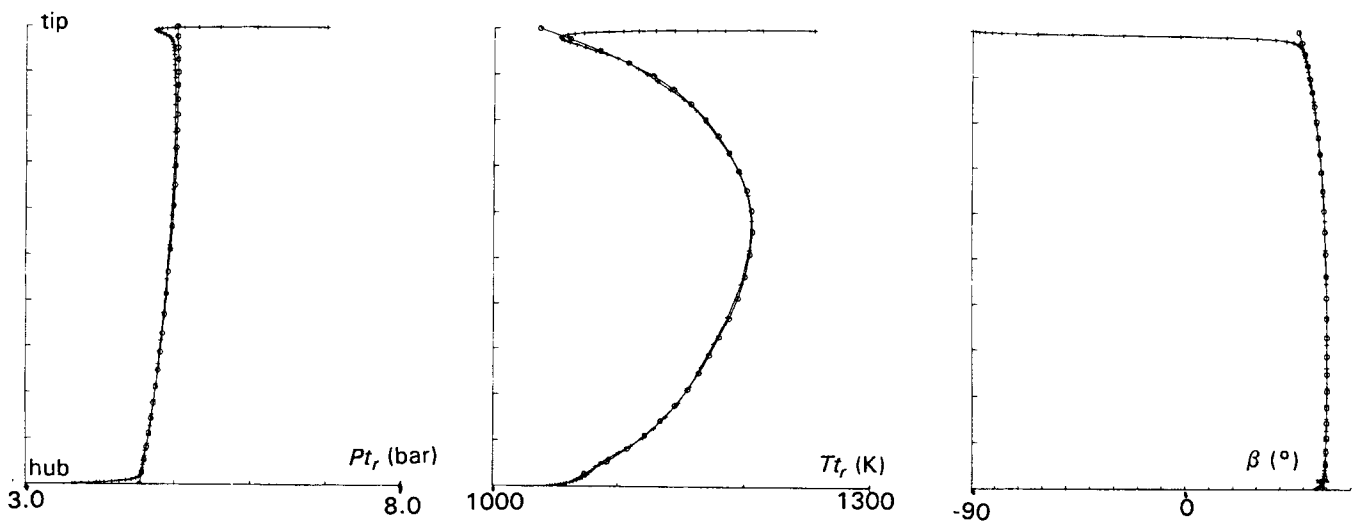

Fig. 8 : Inlet condition profiles

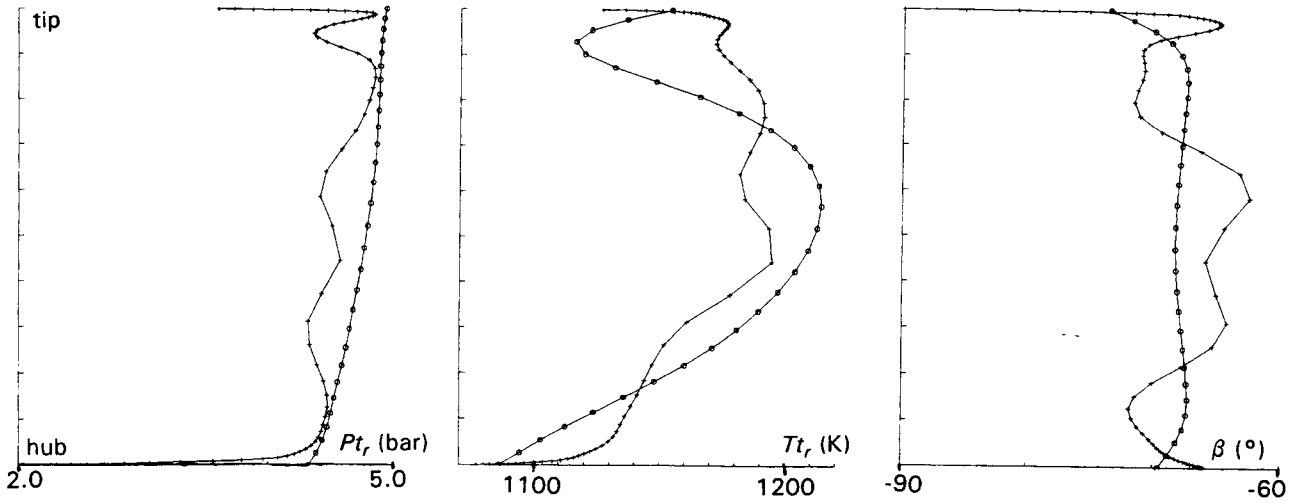

Fig. 9 : Mean distributions in the analysis plane

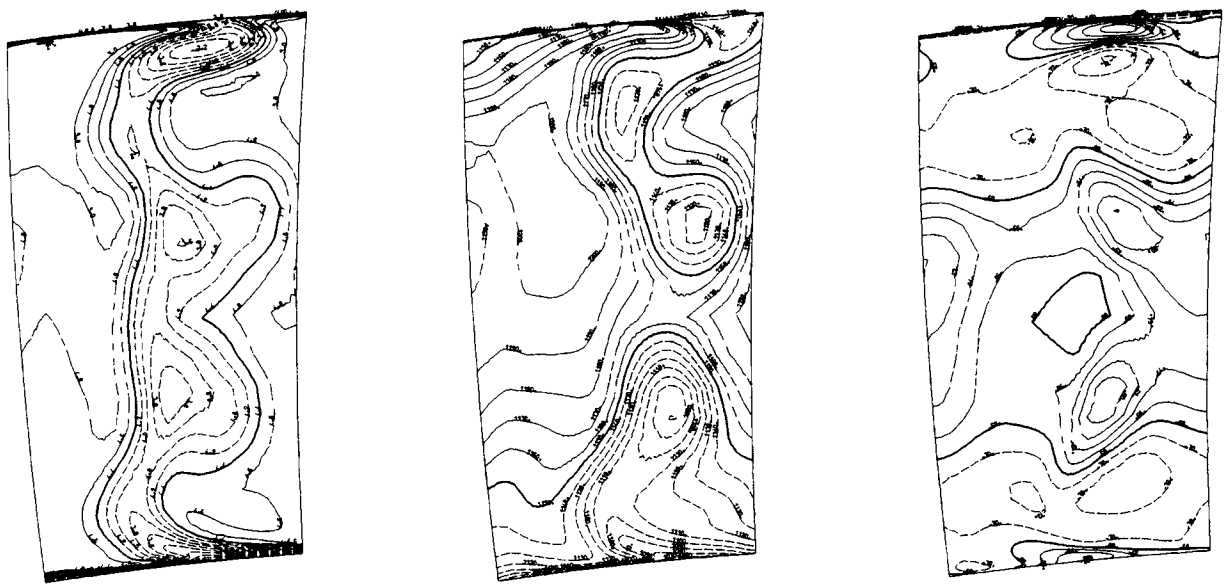

relative stagnation pressure relative stagnation temperature relative flow angle

Fig. 10 : Flow field contours in the analysis plane

Distribution in the Analysis Plane

The radial distributions of mean relative stagnation pressure, stagnation temperature and flow angle in the analysis plane (fig. 9) show the location of at least three vortices. The minima of relative stagnation pressure are situated at about 30, 60, 95% height and correspond to under-turning maxima on the flow angle representation. The temperature distribution in the analysis plane recalls the inlet profile on which analogous variations have been superimposed.

The radial evolutions of pressure, temperature and angle are completed by views of the corresponding two-dimensional distributions of the same scalars in the analysis plane (fig. 10). The previously mentioned loss cores can easily be identified in the 2D representation.

The lack of smoothness of the mean radial distributions in the mid-height region reveals a still insufficient degree of radial discretization in this area, characterized by the complex secondary flows described below.

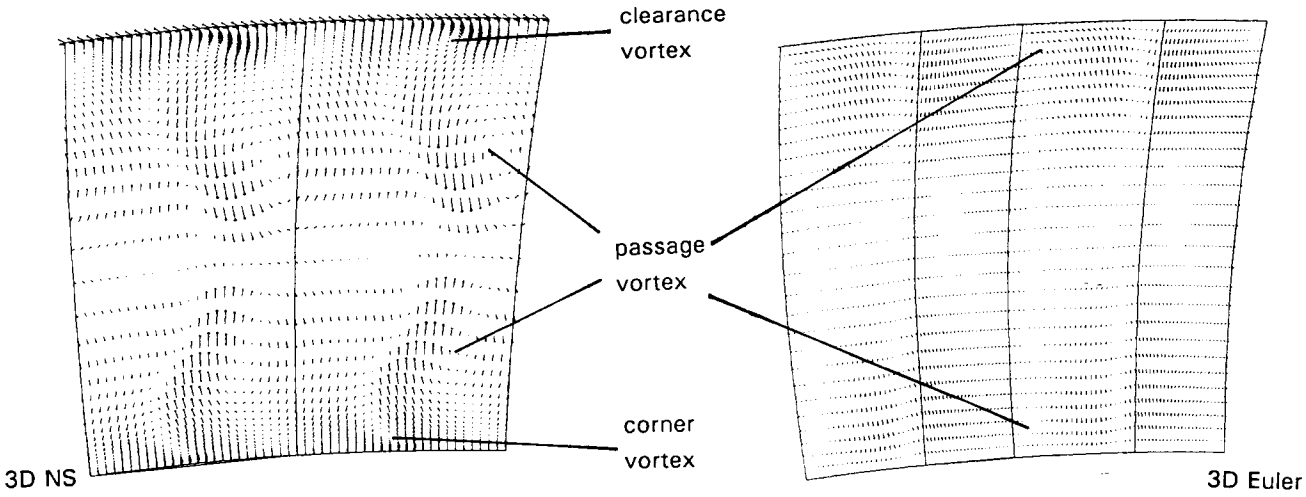

Fig. 11 : Secondary flow velocity vectors in the analysis plane

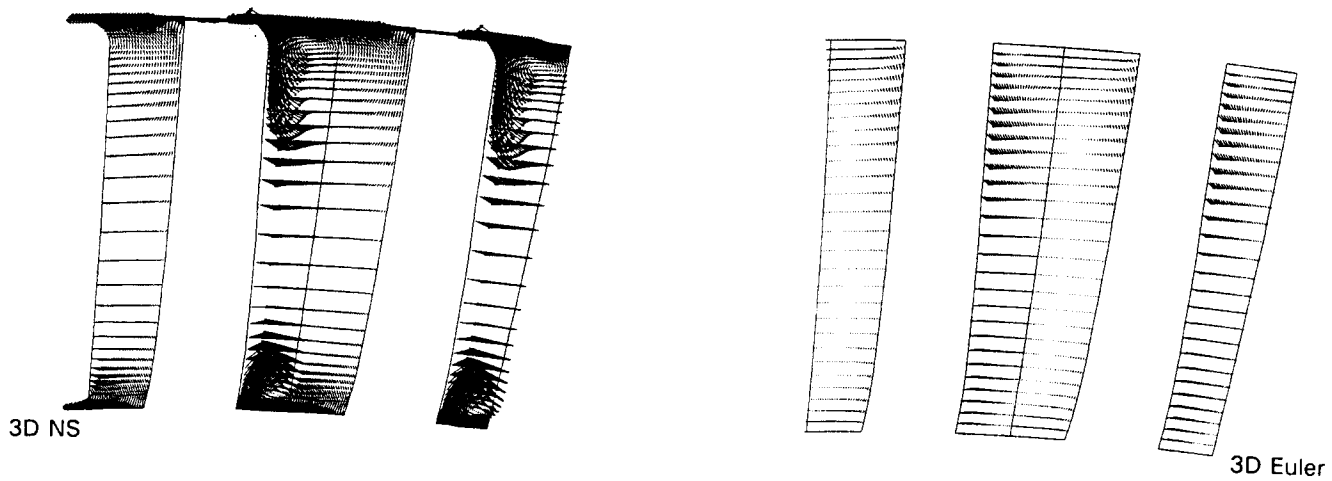

Fig. 12 : Secondary flow velocity vectors in a blade cutting plane

Secondary Flow Velocities

Passage and Corner Vortices. The loss cores appear as vortex centers on the secondary flow velocity representation of fig. 11, and correspond to the well-known passage vortices and to the tip clearance vortex. The two counter-rotating vortices are very close to one another. This leads to the disappearance of any free stream zone and to the coupling of the two vortices, mutually tending to amplify the under-turning in the mid-height region. At root section, a zone of under-turning due to corner vortices is detected. The birth of the passage vortices leading to fluid migration from the endwalls to the mid-height zone along the suction side - the contrary happening on pressure side - is shown in a plane cutting the blade in fig. 12.

The Euler secondary flow pattern shown for the same planes in fig. 11 and 12 reveals passage vorticies of lower intensity than for the Navier-Stokes computation and located closer to the endwalls. They correspond to the slight under-turning maxima of the deviation angle

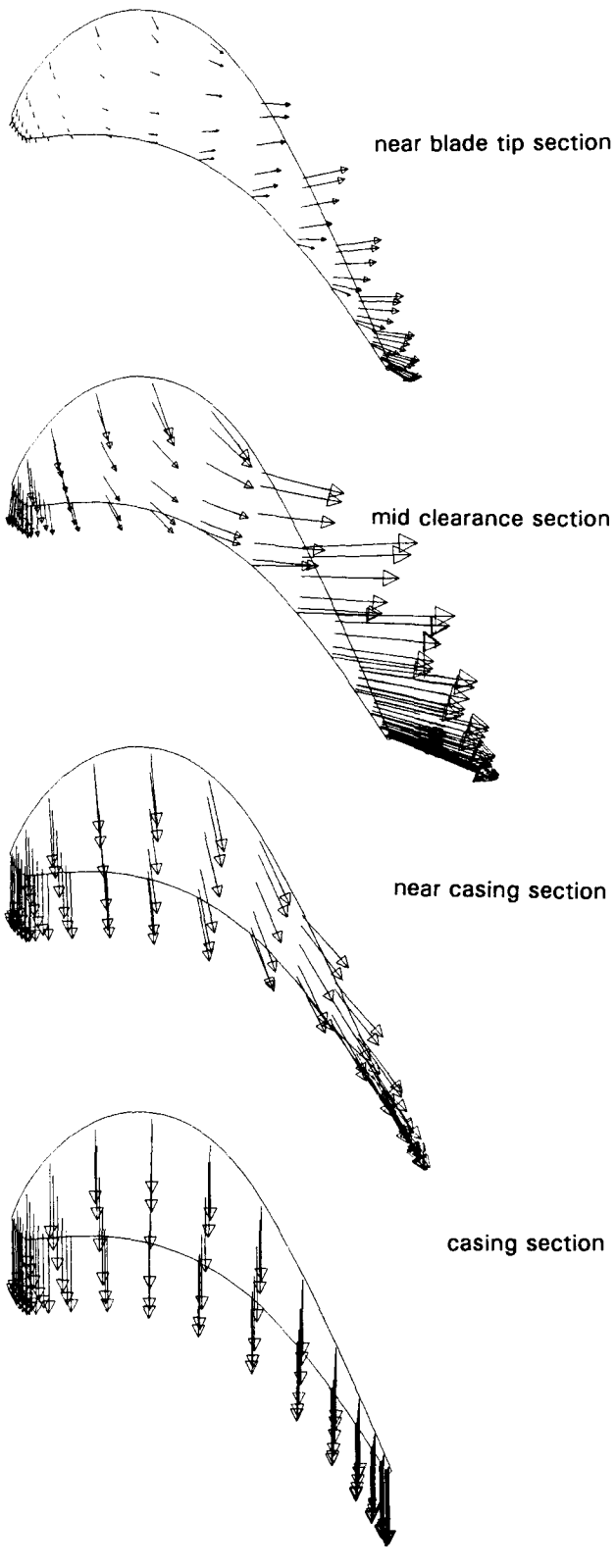

Fig. 13 : Relative velocities in clearance sections

distribution also given for the Euler computation in fig. 9. The much higher intensity of the passage vortices in the Navier-Stokes computation than in the Euler computation can be explained as follows. Passage vorticies are due to incoming vorticity which is quite low for the Euler computation as can be seen on the almost uniform inlet conditions on fig. 8. For the Navier-Stokes computation these conditions are corrected near the endwalls to account for the viscous shear which leads to a higher level of vorticity and thus to stronger secondary flows.

Analysis of the Tip Clearance Region

A sharply defined clockwise vortex near the casing in fig. 11 can be identified as a tip-clearance vortex, resulting in an under-turning zone on the mean angle distribution and a loss core on the pressure distribution. Its origin is due to fluid migration from the pressure side to the suction side in the trailing edge part of the clearance gap.

This migration is displayed by the gap velocity distribution in fig. 13. The radial evolution of relative velocity vectors reveals two opposite flows. In the leading edge part of the gap, fluid migration is occuring from suction to pressure side, due to viscous shearing induced by the stationary casing. At the rear part of the clearance, a pressure-driven flow from pressure to suction side is taking place. This migration is most significant at mid-gap and vanishes at the casing where viscous shear only is present.

This effect is illustrated by the relative Mach number contours shown in fig. 14 for respective heights of 90 and 95%, as well as for blade-tip, mid-clearance and near-casing sections. The deterioration of the flow field due to clearance effect fluid migration appears on the suction side where it extends from the throat to the trailing edge and affects a region between 95% channel height and casing. The pressure side seems less affected by this kind of phenomenon. The Euler flow-field is almost unvarying in the whole tip region. Therefore only the 95% blade-height section is presented here.

The comparison between isentropic relative Mach number evolution along the blade for the Navier-Stokes and Euler computations (fig. 15), reveals that the capture of the reflected shock on the suction side is stronger for the Euler code as expected. On the pressure side the acceleration is identical for both codes. At mid-height, global shapes of the Mach distribution are identical, with lower values for the Navier-Stokes code due to a higher value of static pressure at convergence for this height. A tip clearance effect seen by the Navier-Stokes code is

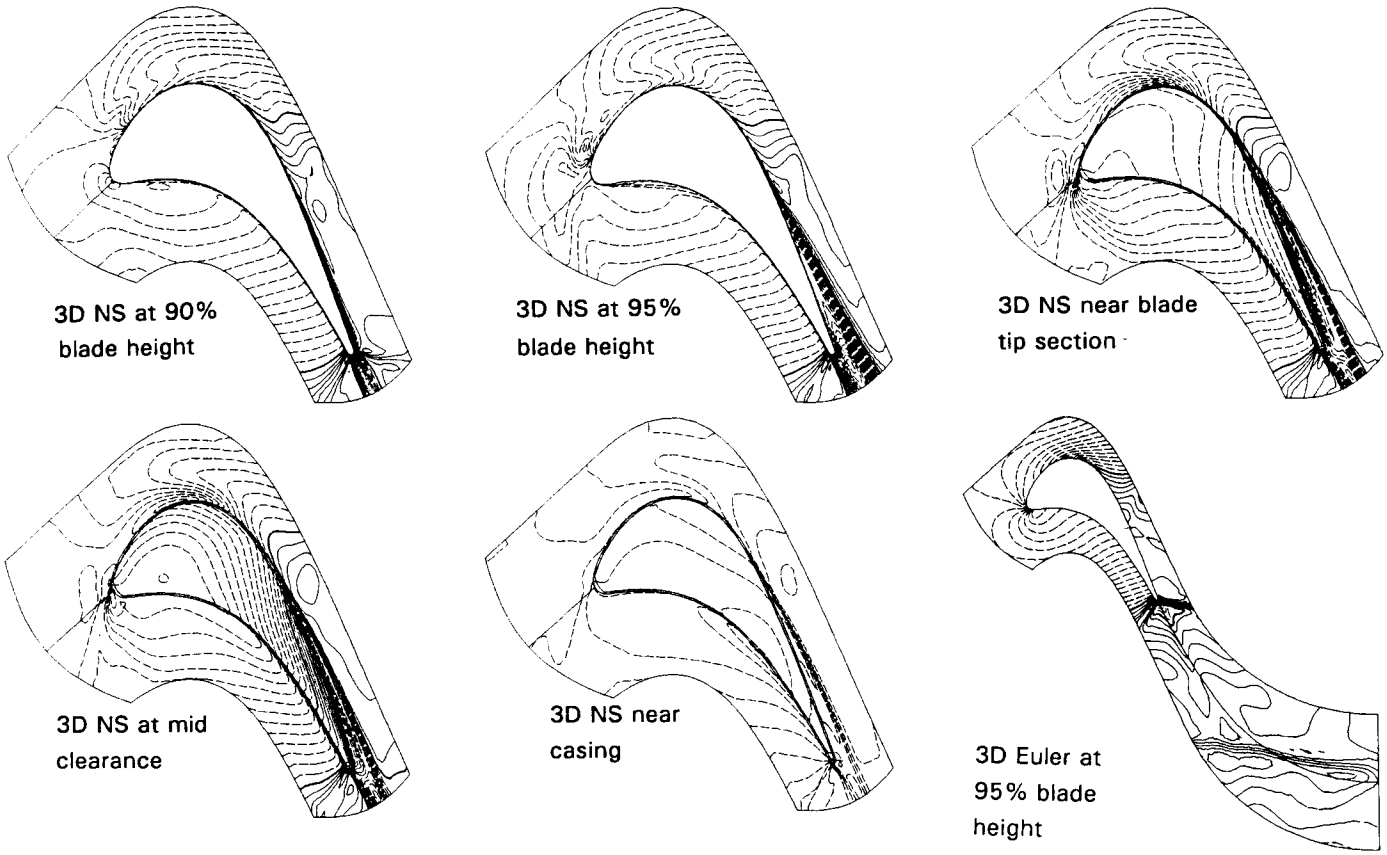

Fig. 14 : Relative Mach number contours ($\Delta Ma_r = 0.05$)

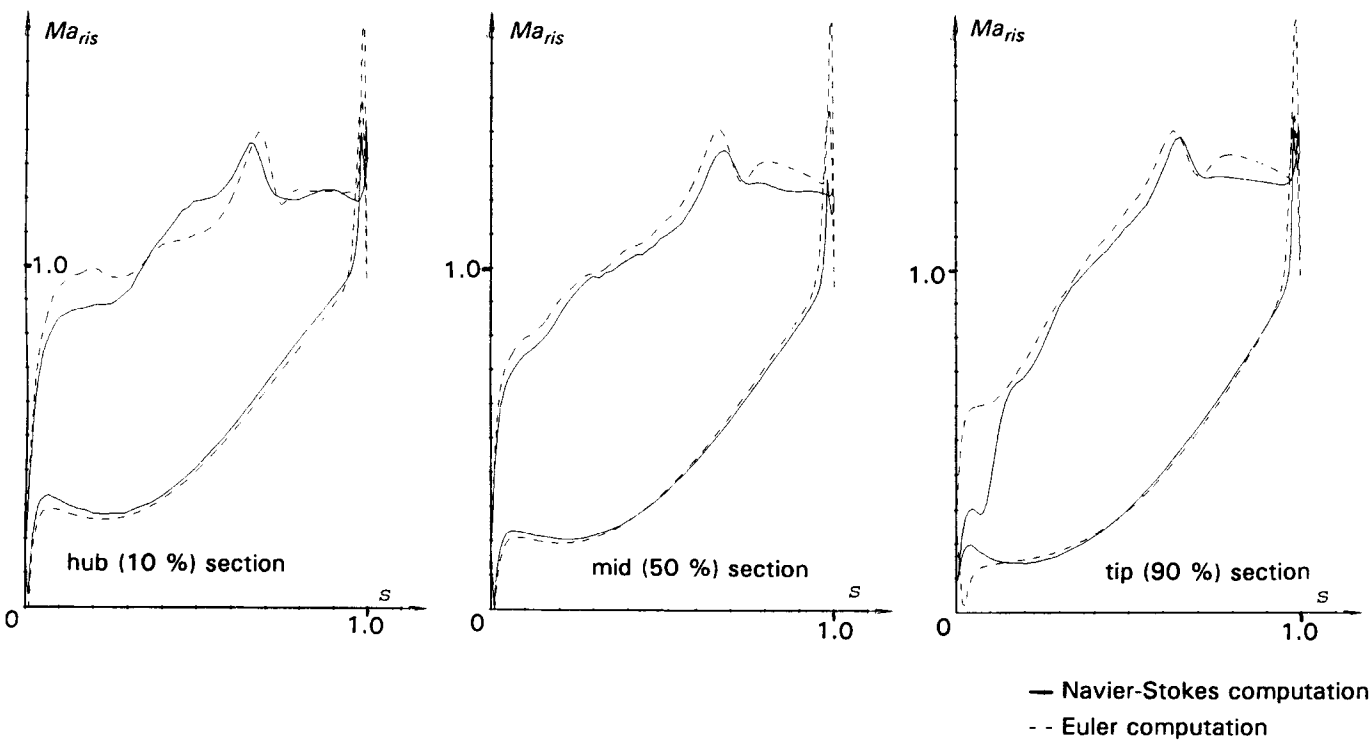

Fig. 15 : Isentropic relative Mach number evolution

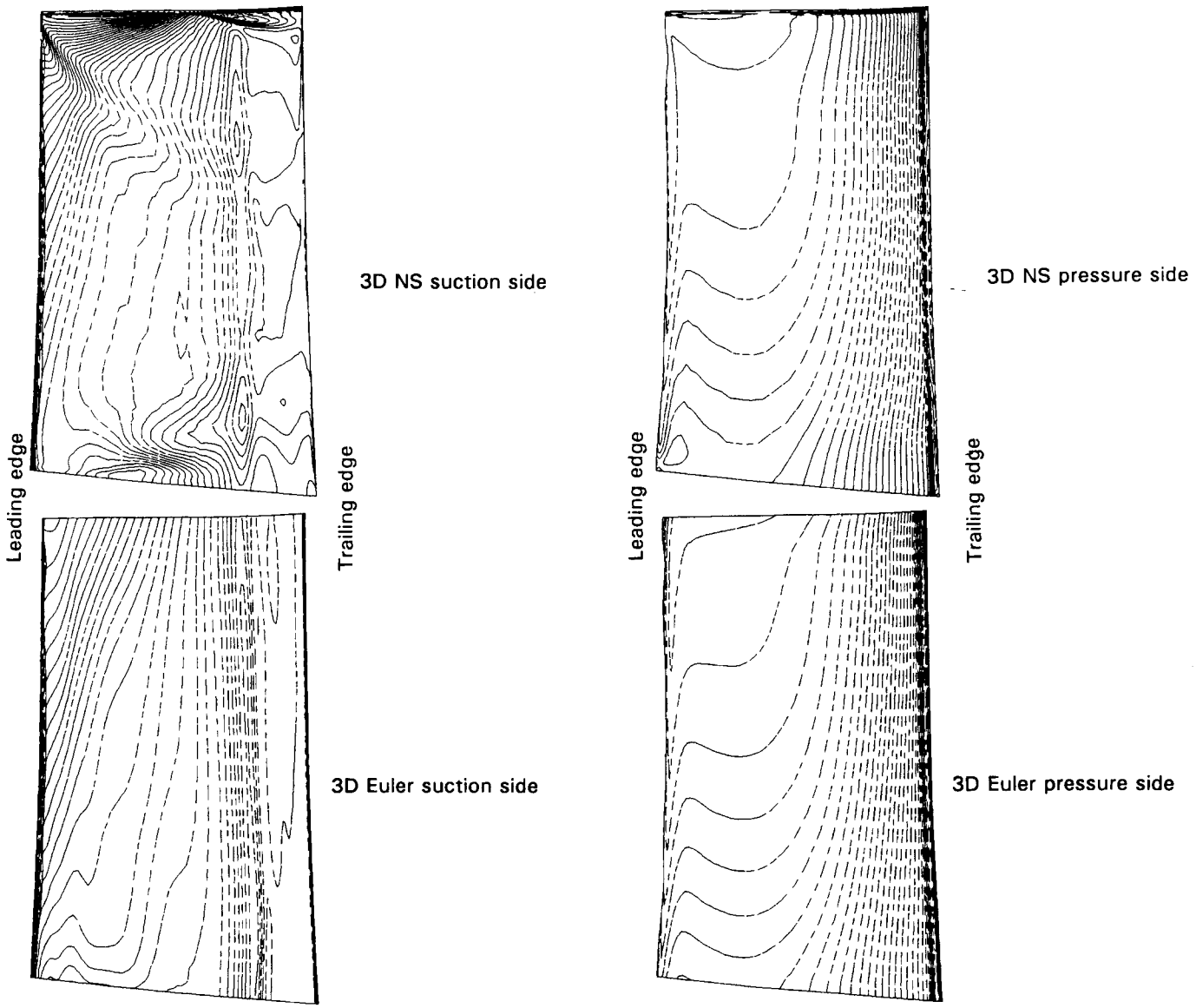

($\Delta P = 0.1$bar)

Fig. 16 : static pressure distribution on the blade

taking place at the leading edge of the suction side tip section resulting in a strong deceleration.

This effect is underlined by strong static pressure gradients in that zone visible on the two-dimensional static pressure distribution (fig. 16). At the trailing edge part of the suction side a perturbated zone is also observed. This region is separated from the previous one, probably due to shock interaction with the clearance. The trailing edge gradient region results from the previously mentioned pressure driven fluid migration which affects about 5% of the blade height. At the pressure side Euler and Navier-Stokes distributions are nearly identical which leads to the conclusion that this side is less affected by tip clearance effects.

Essential Features

The tip clearance thickness was chosen to be representative of actual working conditions of engines. Its value can be considered as very low compared to the tip clearances studied in the case of lower aspect ratio turbines (Liu et al., 1991). However the calculation shows that the extent of the affected region downstream of the blade is about 10% of the total height of the flowpath (fig. 10 and 11). The exit conditions of the rotor are thus

notably modified by the presence of the tip clearance effect. This underlines the importance of including tip clearance modelling in the analysis of rotor blades by 3D Navier-Stokes calculations. The re-distribution of stagnation temperature and pressure profiles is as well of prime importance for the design of the following stator. However the flow features shown in this work have to be considered carefully, the cooling injections having not been taken into account yet.

CONCLUSIONS

A three-dimensional investigation of the flow around a high pressure turbine rotor was performed with a Navier-Stokes solver and an Euler solver. The tip clearance was taken into account in the Navier-Stokes calculation.

A methodology was worked out for the meshing of this type of geometry. The finally chosen five-domain discretization technique allows a high level of automatization.

The implicit residual smoothing technique introduced into the one-step Lax-Wendroff algorithm leads to a significant run time reduction. The CFL numbers used were equal to three. The total CPU-time duration of the calculation is lower than seven hours using the implicit scheme on a CRAY-YMP compared to about fourty hours for a similar calculation with the explicit scheme.

The high number of discretization points (more than 710,000) leads to a precise description of the tip clearance region. However, the radial distribution of the discretization surfaces is too loose in the mid-channel region leading to an insufficient level of accuracy in this area.

The analysis of the flow can be summarized as follows :

1. The two counter-rotating passage vortices greatly influence the main flow, radially redistributing the stagnation temperature and pressure profiles.

2. These two passage-vortices strongly interact with one another leading to a high under-turning of the flow in the mid-height region.

3. Under-turning is detected near the hub, due to the growth of corner vortices.

4. The calculated interaction between leakage and main flow is very important although the height of the gap is lower than 0.73% of blade span. The interaction zone appears right from the leading edge region.

5. No separation zone is detected on the tip of the blade.

6. The leakage flow can be divided into two parts : the main-stream pressure driven flow at the rear part of the clearance and the shroud dominated zone at the front part.

7. The leakage losses calculated at exit have an amplitude equal to those due to passage vortices although being concentrated in the top 10% of the channel.

Even though very detailed results were obtained at the end of this calculation, a thorough validation of the approach using experimental data has to be undertaken in order to provide the designer with a valuable tool for this kind of problem.

For further investigations, the cooling air emitted in the groove as well as the exact geometry of this part of the blade will have to be modelled. The multi-domain approach of the code will be of great help for this purpose.

ACKNOWLEDGEMENTS

The work described in this paper was supported by DRET and STPA. The authors thank Mr. Veysseyre for his suggestions and previous works and Miss Ritoux for her technical support. At last, they are indebted to Mr. Leconte (Student at Ecole Centrale de Paris) for his initial assaults against the difficulties for tip clearance modelling.

REFERENCES

Ameri A.A. and Arnone A., 1992, "Navier-Stokes Turbine Heat Transfer Predictions Using Two-Equations Turbulence closures", *AIAA Paper* 92-3067.

Billonnet G., Couaillier V., Vuillot A.M. and Heider R., 1992, "Analysis of 3D Viscous Flow including Tip Clearance Phenomena in Axial Turbines", *Revue Française de Mécanique*, 1992-3 and -4.

Booth T.C., 1985, "Importance of Tip Clearance Flows in Turbine Design", Lecture Series 1985-05-01, Von Karman Institute for Fluid Dynamics, Rhode-Saint-Genese, Belgium.

Boyle R. and Giel P., 1992, "Three Dimensional Navier Stokes Heat Transfer Predictions for Turbine Blade Rows", *AIAA Paper* 92-3068.

Briley W.R., Roscoe D.V., Gibeling H., Buggeln H.C., Sabnis J.S., Johnson P.D. and Huber F.W., 1991, "Computation of Flow Past a Turbine Blade With and Without Tip Clearance", *ASME Paper* 91-GT-56.

Cambier L., Couaillier V. and Veuillot J.P., 1988, "Numerical solution of the Navier-Stokes Equations by a multi-grid method", *La Recherche Aérospatiale*, English

Edition, N° 1988-2, pp. 23-42.

Cambier L. and Escande B., 1990, "Calculation of a Three-Dimensional Shock Wave Boundary-Layer Interaction", *AIAA Journal*, Vol. 28, Number 11, pp. 1901-1908.

Chevrin P.A. and Vuillez Ch., 1990, "Viscous Flow Computations in Turbomachine Cascades", *ASME Paper* 90-GT-76.

Choi D., 1992, "3D Navier-Stokes Analysis for a tip leakage flow in a low aspect ratio turbine", *AIAA Paper* 92-0395.

Choi D. and Knight C.J., 1991, "A Study on H and O-H Grid Generation and Associated Flow Codes for Gas Turbine 3D Navier-Stokes Analysis". *AIAA Paper* 91-2365.

Couaillier V., 1990, "Multigrid Method for Solving Euler and Navier-Stokes Equations in Two and Three Dimensions", *Proceedings of the 8th GAMM-Conference on Numerical Methods in Fluid Mechanics*, Braunschweig.

Couaillier V., Grenon R. and Liamis N., 1992, Transonic Supersonic Flow Calculations around Aircraft using a Multi-Domain Euler Code, *13th ICNMFD*, Rome 6-10 July.

Couaillier V., Veysseyre Ph. and Vuillot A.M., 1991, "3D Navier-Stokes Computations in Transonic Compressor Bladings", *10th ISABE Symposium*, Nottingham, GB.

Dorney D.J. and Davis R.L., 1992, "Numerical Simulation of Turbine "Hot Spot" Alleviation Using Film cooling", *AIAA Paper* 92-3309

Eriksson L.E., 1984, "Boundary Conditions for Artificial Dissipation Operators", *FFA* TN 1984-53.

Escande B. and Cambier L., 1991, "Validation of the CANARI code by computing the 3-D turbulent flow through a turbine stator". *77th PEP AGARD "CFD Techniques for Propulsion Applications"* San Antonio (USA), May 27-31.

Fourmaux A. and Petot B., 1991, "Three Dimensional Inviscid Compressible Calculations Around Axial Flow Turbine Blades", *10th ISABE Symposium*, Nottingham, GB.

Heyes F.J.G., Hodson H.P. and Dailey G.M., 1991, "The Effect of Blade Tip Geometry on the Tip Leakage Flow in Axial Turbine Cascades", *ASME Paper* 91-GT-135.

Jacquotte O.P. and Cabello J., 1988, "A Variational Method for the Optimization and Adaptation of Grids in Computational Fluid Dynamics", Numerical Grid Generation in Computational Fluid Mechanics 88, *Proceedings of the 2nd International Conference on Numerical Grid Generation in CFD*, Miami-Beach and ONERA TP n°1988-174.

Jameson A. and Schmidt W., 1985, "Some Recent Developments in Numerical Methods for Transonic Flows", *Computer Methods in Applied Mechanics and Engineering* 51, pp. 467-493, North-Holland.

Lerat A., Sidès J. and Daru V., 1982, "An Implicit Finite-Volume Method for Solving the Euler Equations", *Lecture Notes in Physics*, 170, pp. 343-349.

Liu L.S., Minkkinen G. and Bozzola R., 1991, Analytical and Experimental Determination of Tip Clearance Effects in a High Work Turbine Rotor, *ASME Paper* 91-GT-197.

Michel R., Quémard C. and Durand R., 1969, "Application d'un schéma de longueur de mélange à l'étude de couches limites turbulentes", ONERA NT N°154.

Ni R.H., 1982, "A Multiple-Grid Scheme for Solving the Euler Equations", *AIAA Journal*, vol. 20, n°11.

Perrin G., Leboeuf F. and Dawes W.N., 1991, "Analysis of Three-Dimensional Viscous Flows in a Supersonic Axial Flow Compressor Rotor with Emphasis on Tip Leakage Flow", *ASME IGTI*, Cologne.

Petot B. and Fourmaux A., 1992, "Validation of Viscous and Inviscid Computational Methods around Axial Flow Turbine Blades", *Computational Fluid Dynamics '92*, Vol. 2, Ch. Hirch et al.(Editors), pp. 611-618.

Vialonga J., Petot B. and Chiappa T., 1992, "Assessment of a 3D Euler Code for Subsonic Turbine Vane Flows and Study of the Non Radial BLade Stacking", *ASME Paper* 92-GT-63.

Vuillot A.M., 1989, "A Multi-Domain 3-D Euler Solver for Flows in Turbomachines", *Proceedings of the 9th ISABE Symposium*, Athens, Greece.

Wegener D., Escande B., Billonnet G., Lemeur A. and Jourdren C., 1992, "Comparison between two 3D-NS-Codes and Experiment on Turbine Stator", *AIAA Paper* 92-3042.